nature astronomy

SUPPLEMENTARY INFORMATION

VOLUME: 1 | ARTICLE NUMBER: 0091

In the format provided by the authors and unedited.

Spectroscopic confirmation of an ultra-faint galaxy at the epoch of reionization

Supplementary Information

This PDF file contains the Supplementary Material for the manuscript titled: Spectroscopic Confirmation of an Ultra-Faint Galaxy at the Epoch of Reionization. This document contains the following:

Supplementary text and accompanying references
Supplementary Figure 1

Reduction and calibration of the Keck/MOSFIRE spectroscopic data

We targeted MACS1423-z7p64 in the Y-band with two distinct multi-object slit-masks, which were created using the MOSFIRE Automatic GUI-based Mask Application (MAGMA). The slit masks used on 27 May, 2015 (PI Bradač; 2.30 hrs) and 19 March 2016 (PI Trenti; 1.85 hrs) had the same position angle, but some of the filler slits differed between the masks. We noticed an astrometric shift of $\sim 0\farcs1$ between the two mask files created by MAGMA when overlaying them on an *HST* image. This offset is smaller than one MOSFIRE pixel, so we do not expect that it influences our results obtained from stacking the spectra. On 27 May 2015, we employed an ABAB dither pattern with $1\farcs25$ nod offset, and on 19 March 2016 we employed an ABBA dither pattern also with a $1\farcs25$ nod offset. The detection of the line in the two independent reductions demonstrates that its origin is not arising from systematic effects associated with dithering. Individual exposures were 180 seconds in duration during both nights, totaling approximately 2.30 hours on 27 May 2015 and 1.85 hours on 19 March 2016. The data from the two nights were reduced using the most updated version of the publicly available MOSFIRE data reduction pipeline (DRP) as of 19 March 2016. The reduction pipeline differences, stacks, and rectifies the nodded images, creating two-dimensional signal and noise spectra for each individual slit. Spectra from individual nights were reduced separately due to varying observing conditions and differences in the positions of the filler slits.

The average seeing was $0\farcs70$ on 27 May 2015 and $0\farcs85$ on 19 March 2016 in the J-band. Seeing on 27 May 2015 was calculated solely from the J-band alignment images directly preceding Y-band science observations. The seeing was stable on 27 May 2015 throughout our observations, but less stable on 19 March 2016. A bright star on the 19 March 2016 science mask allowed us to track the seeing in the Y-band during our observations, which we then normalized to the J-band seeing. Because the seeing differed between the two observing nights, we smoothed the 27 May 2015 two-dimensional spectra to match the seeing on 19 March 2016 before combining the spectra. The two individual two-dimensional spectra from the observations on 27 May 2015 and 19 March 2016 were combined by an inverse variance-weighted sum at each pixel. The inverse variance spectra were obtained from the two-dimensional noise spectra produced by the MOSFIRE DRP.

The spectra from 27 May 2015, 19 March 2016, and the inverse variance stack of the two are shown in Supplementary Figure 1. A single emission peak is observed in both the 27 May 2015 spectrum and the 19 March 2016 spectrum. The spatial and spectral location of the peak emission is slightly offset between the two observations despite using the same slit-mask setup. However, the offset is consistent with other emission lines in our slit-mask, once we degrade those emission lines to match the S/N of the Lyα line. The two-dimensional stack shown in the bottom panel of Supplementary Figure 1 differs from the one shown in Figure 1. Supplementary Figure 1 shows a direct stack, whereas in Figure 1 we show a cross-correlated stack accounting for the observed vertical and horizontal shift. The cross-correlated spectrum is used for the calculation of the line flux and S/N. The observed wavelength of the Lyα line is measured from the stack in Supplementary Figure 1, which does not incorporate any spatial or spectral shifting.

To extract the one-dimensional spectrum from the two-dimensional co-added spectrum, we used an aperture whose size was chosen to enclose 2*FWHM of the average seeing during the observations. The one-dimensional spectrum shown in Figure 1 was extracted from the co-added two-dimensional spectrum, so the worse seeing was used to define the aperture size. At each point along the spectral axis, pixels within the spatial aperture were summed with weights determined from a gaussian whose width was also determined by the seeing, producing a one-dimensional spectrum. Flux calibration was done by comparing the one-dimensional extracted spectrum of a standard star we observed to a model spectrum of the same spectral type that was observed on a different night but with comparable atmospheric seeing and transparency. This step takes into account the slit-loss for a point source. Before comparison, we scaled the model spectrum to the apparent magnitude of the observed standard, then correct it for the airmass and galactic extinction of our observations. The ratio of the scaled, corrected model spectrum to the observed telluric spectrum represents the sensitivity function of the telescope.

While the flux calibration corrects for slit-loss from a point-source, we expect that the Lyα emission from MACS1423-z7p64 is more extended [1, 2]. The simplest model for the Lyα spatial distribution is that it traces the rest-frame UV-continuum, sampled by the WFC3/IR filters. From the *HST* F125W, F140W and F160W cutouts in Figure 3, it is clear that the source is well-resolved. To estimate the flux lost from the slit due to the extended nature of MACS1423-z7p64 (in addition to the point-source term already accounted for), we compare the flux lost from the $0\farcs7$ MOSFIRE slit for our source versus a point source, both convolved with a Gaussian kernel whose width is determined by the seeing. We model our source with a Sersic profile using GALFIT [3], finding a best-fit Sersic index of ~ 2.7 and effective (half-light) radius of $r_{\rm eff} \sim 1''$ in F140W, the *HST* filter with the highest S/N. We find a slit-loss correction of 1.6; i.e. we multiply our calibrated flux by this factor to account for the additional flux lost due to the extended nature of the source. This correction has been applied to all MOSFIRE flux and equivalent width values reported in the paper.

Two bright galaxies can be seen near the top of the slit in Figure 3. Their traces contaminate both spectra at approximately the same vertical position as the top negative residual from the emission line. We subtracted these traces and their negative residuals by calculating the average pixel value in each row of the reduced two-dimensional spectrum from each night separately. The spectra shown in the top two panels of Supplementary Figure 1 are post-subtraction. The co-added spectrum shown in the bottom panel of Supplementary Figure 1 was obtained from the trace-subtracted individual spectra.

In principle, the continuum from this galaxy could be detected by binning over a sufficiently large bandpass. We note that the negative signals of the aforementioned contaminating galaxies are larger than the continuum predicted from the measured F125W

HST flux, which is red-ward of Lyα without containing any flux from the Lyα line itself. We nonetheless checked for continuum from MACS1423-z7p64 by comparing the means of the one-dimensional spectrum red-ward and blue-ward of the Lyα emission before subtraction of the contamination. When computing the means, we used approximately the same size bandpass red-ward and blue-ward of Lyα ($\sim$ 550Å). Before computing the means we clip off $\sim$ 10% from both ends of the distributions to reject sky line contamination. We do not measure a statistically larger mean red-ward than blue-ward of Lyα, which is evidence that we are not detecting the continuum from MACS1423-z7p64. This is not surprising given the level of the contamination compared to the expected continuum signal.

The S/N of the emission line was determined from the one-dimensional spectrum shown in Figure 1. S is the flux of the line and N is the RMS noise summed in quadrature over the same bandpass used to determine the flux, which is $10501 - 10510$Å. The line flux is $0.41 \pm 0.06 \times 10^{-17}$ erg/cm^2/s, resulting in a $S/N = 6.7$ detection. The bandpass is limited on the red side due to the sky line as shown in Figure 1. The sky line renders an asymmetry test unreliable and also potentially reduces the line flux we are able to measure. The Lyα detection is not sensitive to the pixel contributing a significant amount of flux just blueward of the sky line in Figure 1; the S/N is 6.0 if this pixel is not included in the bandpass. The emission line at 10504Å is the only $S/N > 5$ feature within the $\pm$50Å window from GLASS that appears in both the 27 May 2015 and 19 Mar 2016 spectra.

Description of the GLASS data

GLASS is an *HST* large program that targeted 10 massive galaxy clusters during Cycle 21 [4, 5]. Data were taken with the WFC3 G102 and G141 grisms in the cluster cores and the ACS G800L grism in parallel fields. Because we focus on the cluster core in this work, we only use the data from the WFC3 grisms. 14 orbits were allocated for each cluster, distributed to achieve uniform sensitivity over the range in wavelengths $0.8 - 1.7\mu m$. Each cluster was observed at two position angles (P.A.s) approximately 90 degrees apart to aid in contamination subtraction. The two GLASS P.A.s for MACS J1423.8+2404 (P.A.= 8° and P.A.= 88°) are shown in Figure 3.

The spectral extraction for MACS1423-z7p64 we performed is similar to that described by [6], but with two important differences that resulted in a slight enhancement in the S/N of the Lyα emission line ($S/N = 2.4$ in this work versus $S/N = 2.1$ from [6]). First, we used an updated reduction of the GLASS data. This is based on a more reliable detection and flux scaling of contaminating sources affecting the flux levels and noise properties of the contamination-subtracted spectra from which the line flux is estimated. Second, we force-extracted the spectrum at the exact coordinates of the source, and in doing so assumed a circular aperture for contamination modeling. In [6], we extracted the spectra using SExtractor-defined segmentation maps of the nearest matches to the coordinates of the object.

The G102 and G141 spectra at both P.A.s are shown in Figure 2. Lyα is detected marginally at $S/N = 2.4$ in the P.A.= 88° G102 spectrum at 10500 ± 50Å, implying a redshift of $z = 7.64 \pm 0.04$, in agreement with the redshift measured with Keck/MOSFIRE. The inferred Lyα equivalent width from GLASS is $W_{\mathrm{Ly}\alpha} = 27 \pm 11$Å. Because the continuum was not detected in the spectrum, the continuum flux density used for the equivalent width measurement was estimated from the broadband *HST* flux in the F125W band. This band was chosen because it samples the rest-frame UV continuum near the Lyα wavelength without containing any contribution from the Lyα emission or the Lyα break.

The G141 spectral coverage allows us to search for additional emission lines at $z = 7.640 \pm 0.001$, such as C IV$\lambda\lambda$1548, 1551 and C III]$\lambda\lambda$1907, 1909, both of which would be blended in the GLASS spectroscopy. No significant spectral features were recovered from this search. The 3σ limits on the fluxes and equivalent widths for C IV and C III] are shown in Table 1. The continuum flux densities used to determine the equivalent widths were estimated in a similar manner to the Lyα equivalent width measurement described above, but instead the F160W and F140W filter fluxes were used for C IV and C III], respectively.

Nominally, the Lyα flux derived from the grism is a factor of ~ 3 larger than the Keck/MOSFIRE flux. However, the grism-derived flux we report in Table 1 was obtained using an aperture designed to optimize the signal to noise ratio (S/N) of the line, whereas the aperture of the MOSFIRE observations is fixed by the size of the slit, 0.″7. Once the apertures are matched, the fluxes from the grism and MOSFIRE agree within the uncertainties. Higher levels of contamination are the most likely cause for the non-detection of Lyα in P.A.= 8° of the grism.

Alternative interpretations of the emission line

We find that the most likely interpretation of the emission line is Lyα at $z = 7.640$. However, we explore the next most likely scenario in which the line is [O II]$\lambda\lambda$3726, 3729 at $z = 1.818$. The strong break observed in the photometry at $\sim 1.05\,\mu m$ rules out emission lines other than Lyα and [O II] since it is either the Lyman or Balmer break. The resolution of MOSFIRE is sufficient to resolve the [O II] doublet at $z = 1.818$. Supplementary Figure 1 shows the expected locations of the 3726Å and 3729Å lines in the [O II] doublet if the emission line observed at $\sim$ 10504Å was the 3729Å line or the 3726Å line, respectively. If the line at $\sim$ 10504Å was the 3729Å line, then the bluer 3726Å line would have been observed since it falls in a region free of strong sky emission lines. The typical 3729Å /3276Å intensity ratio for star-forming galaxies is 1.5/1, so the 3726Å line would have been detected in this case. If the line at $\sim$ 10504Å was the 3726Å line, then the redder 3729Å line would have fallen on a sky line and would therefore have been undetectable.

The strongest evidence against the line being [O II] comes from the grism observations. The GLASS grism spectra cover the [O III] pair in the case where the emission line at $\sim$ 10504Å is [O II]. However, the [O III] pair is not detected in either P.A. (Figure 2), resulting in a 2σ upper limit of $f_{[\mathrm{O\,III}]}/f_{[\mathrm{O\,II}]} < 0.65$ in P.A.=88°. At $z = 1.818$, the galaxy would have an intrinsic stellar mass of $\sim 1 \times 10^9 M_\odot$, which would imply $f_{[\mathrm{O\,III}]}/f_{[\mathrm{O\,II}]} \geq 1.5$

[7], inconsistent with our observations. Furthermore, the SED fitting strongly prefers the $z = 7.640$ solution ($\chi^2_\nu = 0.9$) over the $z = 1.818$ solution ($\chi^2_\nu = 3.4$). In summary, we are confident that the line at ~ 10504Å is not [O II] and therefore must be Lyα.

Supplementary References

1. Steidel, C. C. *et al.* Diffuse Lyα Emitting Halos: A Generic Property of High-redshift Star-forming Galaxies. *Astrophys. J.* **736,** 160 (2011).
2. Wisotzki, L. *et al.* Extended Lyman α haloes around individual high-redshift galaxies revealed by MUSE. *Astron. Astrophys.* **587,** A98 (2016).
3. Peng, C. Y., Ho, L. C., Impey, C. D. & Rix, H.-W. Detailed Decomposition of Galaxy Images. II. Beyond Axisymmetric Models. *Astron. J.* **139,** 2097–2129 (2010).
4. Schmidt, K. B. *et al.* Through the Looking GLASS: HST Spectroscopy of Faint Galaxies Lensed by the Frontier Fields Cluster MACSJ0717.5+3745. *Astrophys. J.* **782,** L36 (2014).
5. Treu, T. *et al.* The Grism Lens-Amplified Survey from Space (GLASS). I. Survey Overview and First Data Release. *Astrophys. J.* **812,** 114 (2015).
6. Schmidt, K. B. *et al.* The Grism Lens-Amplified Survey from Space (GLASS). III. A Census of Lyα Emission at $z \gtrsim 7$ from HST Spectroscopy. *Astrophys. J.* **818,** 38 (2016).
7. Henry, A. *et al.* Low Masses and High Redshifts: The Evolution of the Mass-Metallicity Relation. *Astrophys. J.* **776,** L27 (2013).

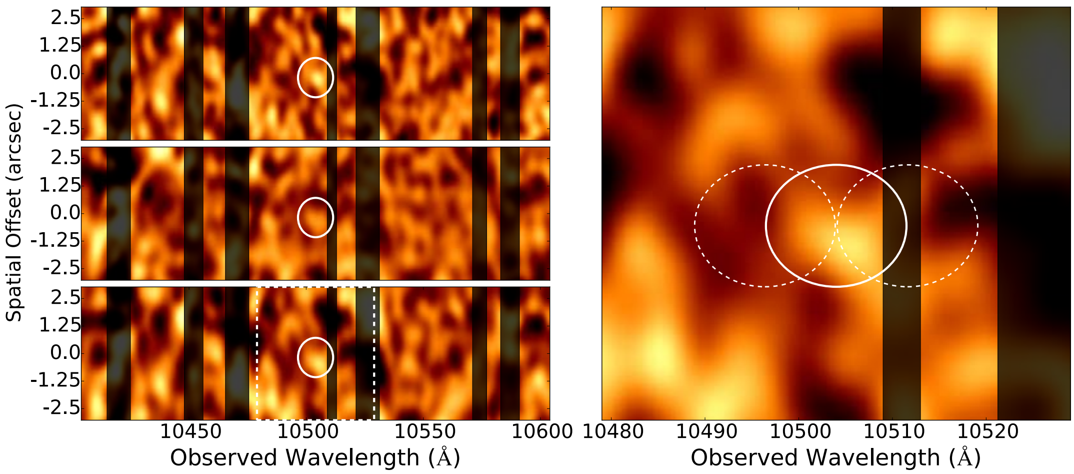

Supplementary Figure 1: Two-dimensional signal spectra from the (**Top left**) 2.30 hr 27 May 2015 observation, (**Middle left**) 1.85 hr 19 March 2016 observation and (**Bottom left**) direct inverse-variance stack of the two spectra. The emission line, which we are confident is the Lyα line, is circled in white in all panels. (**Right**) Zoomed in region on the emission line from the stacked spectrum shown in the bottom left panel. Again, the emission line at 10504Å is circled in white. The dotted circle to the left (right) of the emission line shows the expected location of the 3726Å (3729Å) line in the [O II]$\lambda\lambda$3726, 3279Å doublet if the observed emission line was instead the 3729Å (3726Å) line at $z = 1.818$. The observed emission line at 10504Å cannot be the 3729Å line because we would have detected the bluer 3726Å line in that case. In the case that the observed emission line at 10504Å was the 3726Å line, the sky line would have obscured the 3729Å line. The grism spectra provide strong evidence against the [O II] interpretation of the line, however. The spectra in all panels have been smoothed to the average seeing of each observation using a circular Gaussian kernel.